Geomorphology 404 (2022) 108186

Contents lists available at ScienceDirect

Geomorphology

journal homepage: www.journals.elsevier.com/geomorphology

Capturing the complexity of soil evolution: Heterogeneities in rock cover and chemical weathering in Montana's Rocky Mountains

Sarah S. Benjaram [a], Jean L. Dixon [a,*], Andrew C. Wilcox [b]

[a] Department of Earth Sciences and the Institute for Ecosystems, Traphagen Hall 216, Montana State University, Bozeman, MT 59717-3480, United States of America
[b] Department of Geosciences, Charles H Clapp Building 357, University of Montana, Missoula, MT 59812, United States of America

ARTICLE INFO

Keywords:
Soil
Chemical weathering
Hillslopes
Rock-cover
Soil thickness
Critical zone

ABSTRACT

We investigate the relationship between chemical weathering, persistence of soil cover, and topography in two neighboring mountain ranges in the northern Rockies of western Montana, USA. We augment existing tools for measuring chemical weathering with adjustments for both local and landscape-scale contributions from unweathered rock fragments, boulders, and bedrock exposure. Adjusted weathering intensities recognize that quantifying weathering in mountainous systems should account for rock exposure, rather than focusing solely on fine-grained soil mantles. Our study systems' distinct morphologies are shaped by their unique climate histories. The previously glaciated Bitterroot Mountains consist of steep hillslopes with abundant rock cover, while the neighboring unglaciated Sapphire Mountains display convex, soil-mantled hillslopes. Over 380 soil thickness measurements, 118 analyses of soil and rock geochemistry, and digital terrain analysis reveal that patchy soils in the bedrock-rich system are roughly half as thick as those in the continuously-soil-mantled landscape, and ~45% less weathered, despite wetter conditions that would be expected to enhance weathering. These disparities increase when accounting for coarse rock fragments in soils and bedrock cover across the study catchments. The near continuously soil-mantled Sapphire system experiences ~1.5 times greater weathering intensity at a catchment scale compared to the bedrock-rich Bitterroot system. Rock exposure across the mountainous study system increases with increasing slope gradient. However, we find no clear threshold at which soils decrease in abundance or weathering intensity, and soils are surprisingly resilient even at the steepest hillslopes (comprising ~60% of the landscape area at slopes >30°). Our new data quantify soil abundance and chemical weathering intensity at both local and landscape scales. This work highlights how measurements of soil and rock cover need to be incorporated into studies quantifying chemical weathering, as traditional approaches may significantly overestimate and mischaracterize weathering regimes in mountain environments.

1. Introduction

In mountainous landscapes, chemical weathering is thought to play a key role in influencing the availability of rock-derived nutrients to ecosystems (Hahm et al., 2014), controlling thresholds for soil cover (Dixon and von Blanckenburg, 2012; Riebe et al., 2017), and regulating the long-term drawdown of atmospheric CO_2 (e.g., Berner et al., 1983; Walker et al., 1981; West, 2012; Maher and Chamberlain, 2014). But investigating weathering and its governing controls in many mountain systems is complicated and challenging due to heterogeneous regolith and surface cover and strong topographic and hydrologic variability.

Local regolith and soil, landslides deposits, and bedrock surfaces all contribute to weathering in complex mountain terrain (e.g., Emberson et al., 2016). Stream solute fluxes may integrate across these disparate signals, but solute measurements reflect short temporal scales that may miss longer-term processes or variability. Measurements of the chemistry of residual soils, on the other hand, provide longer-term but highly local insights. These soil-chemistry measurements are sometimes used to make broad inferences regarding the weathering regime of heterogenous mountainous systems (e.g., Dixon and von Blanckenburg, 2012; Larsen et al., 2014).

In the critical zone of a dynamic hillslope, the chemical alteration and dissolution of bedrock (from millimeters to tens of meters below the surface) produce regolith, the unconsolidated material at Earth's surface. In the terminology used throughout this manuscript, the *regolith* is composed of *soil*, the surface mantle of mobile material, and in some

* Corresponding author at: Montana State University, United States of America.
E-mail address: jean.dixon@montana.edu (J.L. Dixon).

https://doi.org/10.1016/j.geomorph.2022.108186
Received 11 September 2018; Received in revised form 23 February 2022; Accepted 28 February 2022
Available online 3 March 2022

cases *saprolite*, the physically immobile but chemically-altered and weathered material underlying soils. Saprolite retains its relict rock structure even as weatherable constituents are removed in solution. Soil is produced at its base by the disruption of saprolite and/or bedrock by physical mechanisms such as tree throw, bioturbation, and frost cracking that mobilize underlying material and further enhance chemical weathering, or at the surface by dust deposition and transport from upslope. In this way, the mineral grains that are found in unconsolidated mantles at much of Earth's surface started as part of the underlying or upslope parent rock, were exhumed from depth, chemically and physically altered into soils and saprolite, and then either left in-situ or transported by dust and/or downslope processes to their present location.

In some systems, much of the surface may appear devoid of regolith, even while chemical weathering, regolith production, and erosion processes are ongoing. Patchy soils and exposed rock in steep mountainous landscapes may reflect local outpacing of rock comminution and soil production by physical erosion (e.g. Heimsath et al., 2012). However, if and at what rate a limit of soil production exists is debated and may be specific to each landscape (Dixon and von Blanckenburg, 2012; Heimsath et al., 2012), and likely depends partly on rock strength and climate (Pelletier and Rasmussen, 2009; Perron, 2017). This limit may be inferred in weathering rates and the landscape-scale exposure of bedrock in mountain systems (Dixon and von Blanckenburg, 2012), but it is surprisingly elusive at a local scale. For example, several studies have found that soil production rates in steep mountain systems keep pace with regional erosion rates (Heimsath et al., 2012), despite the fact that such soils may become highly localized as bedrock cover increases. Landscape-scale transitions from a soil-mantled system to one of increasing bedrock-exposure are thus not easily explained by simple erosional thresholds, though local exposures of soil and rock may vary with topography (DiBiase et al., 2012; Milodowski et al., 2015).

Research has flourished on chemical weathering in soil-mantled and creep-dominated terrains (Burke et al., 2007; Yoo et al., 2007; Lebedeva and Brantley, 2013; Ben-Asher et al., 2021), resulting in several unifying models for how soils evolve during bedrock weathering and physical erosion (Anderson et al., 2007, 2019; Mudd et al., 2013; Brantley et al., 2017). Though soil development and regolith weathering have been quantified in steep landscapes, studies tend to focus on soil-mantled portions of the system that fit within the above models and associated sampling designs (e.g., Riebe et al., 2004; Dixon et al., 2012). A solely regolith-focused perspective, however, would provide limited insight into long-term chemical weathering in landscapes with abundant bedrock.

The exposure of bare rock has important implications for chemical weathering processes. Chemical weathering rates are set by a combination of factors, including but not limited to physical erosion rate (Stallard and Edmond, 1983; Riebe et al., 2001, 2003, 2004; Green et al., 2006; Yoo et al., 2007; Burke et al., 2009; Dixon et al., 2009b), lithology, rock chemistry (Garrels and Mackenzie, 1971; Meybeck, 1987; Bluth and Kump, 1994; Edmond et al., 1996), and moisture availability (Bluth and Kump, 1994; White and Blum, 1995; Dixon et al., 2016). Physical erosion and chemical weathering rates are positively correlated across diverse landscapes, since physical erosion refreshes the supply of unweathered material from below and weathering reactions increase erodibility (e.g., Anderson et al., 2002; Riebe et al., 2004; West et al., 2005; Burke et al., 2009; Dixon and von Blanckenburg, 2012). Weathering in such systems is largely referred to as *supply-limited*, because weathering rates keep pace with erosion and are limited primarily by the supply of fresh minerals (Stallard, 1985; West et al., 2005), resulting in soils with similar and high chemical depletions regardless of erosion rate (Ferrier et al., 2016). By contrast, in *kinetically-limited* systems mineral supply rates result in diminishing returns to chemical weathering as there is insufficient time, water, or acidity to deplete weatherable minerals (Ferrier and Kirchner, 2008; Gabet and Mudd, 2009). In systems with abundant bedrock at the surface, chemical weathering rates may be decoupled from mineral supply rates, either because of high erosion rates, so that mineral residence times are brief, or because of dry conditions, if moisture is insufficient for weathering reactions to progress (Rasmussen et al., 2011).

Previous work suggests limits to regolith production may determine the transition from supply to kinetic limitation (e.g., Anderson et al., 2019; Dixon and von Blanckenburg, 2012; Fletcher et al., 2006) or set maximum weathering rates (Ferrier and Kirchner, 2008). Despite this, the spatial variability of rock cover within soils and across the landscape has not explicitly been incorporated into chemical weathering studies. We anticipate that this bias in perspective results in overestimations of surface weathering intensities and fluxes from mountainous or rocky landscapes.

Improved mechanistic understanding of the controls on soil and bedrock cover and their influence on chemical weathering in mountain systems is still needed. Understanding the extent of surface weathering in heterogeneous, rocky landscapes requires quantifying the spatial variability of soil, variation in weathering extent, and the complex controls on both. To address these challenges, we pursue the following objectives in two adjacent mountainous systems with disparate glacial histories: 1) to quantify the amount of soil and bedrock cover at local (1 m) to landscape (1 km) scales, and 2) to measure the magnitude and variability of chemical weathering intensity in soils. We thus aim to quantify the contribution of soils, rock fragments, boulders, and exposed bedrock to total landscape weathering.

2. Study area

This study draws on the morphologic legacy left by Pleistocene glaciation in the northern Rockies, which provides an ideal natural laboratory for investigating the controls on weathering and soil cover in two disparate mountain landscapes. We focus on two north-south trending mountain ranges, the Bitterroot and Sapphire Mountains,

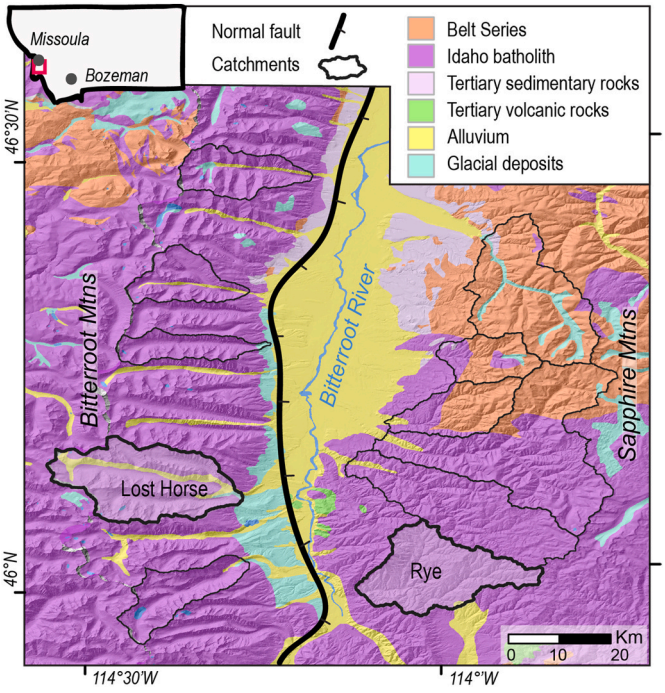

Fig. 1. Study area in western Montana, USA, showing lithology, topographic variability between the Bitterroot and Sapphire Mountains, and catchments selected for topographic analysis. Detailed study sites (Lost Horse and Rye Creeks) have bold outlines. Lithologic basemap from MBMG 1:100k Seamless Geodatabase, a combination of legacy geologic maps, some of which were previously published by the USGS.

which flank the Bitterroot River valley in western Montana (Fig. 1), in the headwaters of the Columbia River basin. These two systems provide contrasts in glaciation history, topography, and soil and rock cover that facilitate investigation of morphology, weathering, and erosion processes.

The Bitterroot and Sapphire Ranges are separated by the 500–1500 m thick east-dipping Bitterroot mylonite shear zone. On the west side of the Bitterroot River basin, the Bitterroot Mountains are underlain by the Idaho batholith, a metamorphic core complex made up of metasedimentary rocks in the north and granitic rocks to the south (Lonn and Berg, 1996; Lewis, 1998). The Bitterroot Mountains primarily comprise late Cretaceous to Eocene granodiorite, quartz monzonite, and granite, including quartz, orthoclase, oligoclase, and biotite, with a coarse-grained to porphyritic texture (Ross, 1950; Foster et al., 2001). The Sapphire Mountains on the east side of the Bitterroot River basin are largely underlain by the Belt Supergroup, a Proterozoic fine-grained metasedimentary and mafic intrusive assemblage. Granitic plutons are scattered throughout, more densely toward the southern end of the block (Hyndman, 1980). Similar modern tectonic forcings are thought to control the ranges bordering the Bitterroot Valley, as the massive granite assemblage underlying them is free of structural or lithologic variations (Lonn and Berg, 1996; Lewis, 1998). Though it has been reported that rock uplift rates are negligible in this vicinity (Foster and Raza, 2002), late Quaternary surface ruptures are visible along Bitterroot front range faults (Stickney, 2014). These active structures may contribute to the contrast in average relief between the two ranges (Fig. 1).

Our work builds on previous investigations of the classically post-glacial topography of the Bitterroot Range (Naylor and Gabet, 2007; Foster et al., 2008; Pederson and Egholm, 2013). The Bitterroot Mountains experienced multiple Pleistocene glaciations (Alden, 1953; Weber, 1972). Glaciers were likely larger in the southern portion of the Bitterroot Mountains, where they extended beyond their valleys and left moraines in the Bitterroot River valley (Weber, 1972). Reconstructions of late Pleistocene weather patterns suggest that Last Glacial Maximum (LGM) precipitation should have been similar across the Bitterroot Range due to the dominating influence of anticyclonic easterlies (Kutzbach and Ruddiman, 1993; Hostetler and Clark, 1997). Naylor and Gabet (2007) noted asymmetry in east-west striking basins of the Bitterroot, likely driven by less solar insolation on north-facing slopes that resulted in enhanced glacial erosion processes. The Sapphire Mountains were either entirely or largely not glaciated, likely due to their lower mean elevation and precipitation rates. Isolated glacial deposits have been mapped in the upper reaches of some high-elevation watersheds in the Sapphires (Fig 1; MBMG seamless), though they are not recognized in all maps (e.g. Lonn et al., 2003).

The Bitterroots receive more modern precipitation than the Sapphires. Weather systems in the study area tend to travel eastward from the Pacific Ocean, depositing nearly three times as much winter precipitation on the western side of the range compared to the eastern side (Whitlock and Bartlein, 1993). Within the Bitterroot Mountains, modern precipitation varies from ~180 cm y^{-1} in our upper study area to ~100 cm y^{-1} in lower parts of the mountains. By comparison, precipitation in the Bitterroot River valley at the base of the range averages 30 cm y^{-1}, and the Sapphires to the east receive 30–130 cm y^{-1}, increasing with elevation (PRISM, 2014 30-year normals). Both ranges are subject to wildfires. Extensive, high-severity fires in 2000 produced debris flows in isolated portions of the Sapphires (Parrett et al., 2004; Hoffman and Gabet, 2007; Gabet and Bookter, 2008; Hyde et al., 2014), though how wildfire influences long-term erosional processes in both mountain ranges is unknown.

3. Approach and methods

Our study combines topographic analysis, laboratory-based measurements of soil chemistry, and field-based analysis of soil cover and thickness to determine how soil formation varies across the study region. We select two representative catchments, Rye Creek (Sapphire Mountains) and Lost Horse Creek (Bitterroot Mountains) for detailed analysis (Fig. 1). These catchments are underlain by the same unit of granodiorite bedrock. We can thus treat lithology as constant between our two study basins, helping to isolate the role of catchment morphology on soil formation. We measure soil distribution and chemical weathering extent across these two catchments by quantifying soil cover and thickness, and through geochemical analyses of soil and rock samples.

3.1. Field methods and sampling

In summer and fall of 2015 and 2016, we sampled soils and bedrock for chemical weathering analysis, and measured soil thickness, spatial cover, and the extent of rock fragments and bedrock exposure. Our sample design was intended to quantify soil cover and chemical weathering intensity across multiple spatial scales and geomorphic settings. To do so, we targeted sample sites at a variety of topographic positions, including hillslopes and valley bottoms at a range of slope gradients and aspects (sites detailed in supplementary material). In this study, regolith is determined functionally as disruptable and augerable material, while the soil subcomponent lacks relict rock structure. Regolith thickness was measured by hand auger to the depth of refusal at 387 points across Rye and Lost Horse Creek catchments. At Lost Horse nearly all augers contacted with coherent bedrock, while in many sites at Rye Creek soils lie atop saprolite. In these cases, soil thickness was determined by the depth at which relict structures from bedrock can be viewed within the weathered sample. Auger sites at Lost Horse Creek were focused on the lower elevation portions of the catchment, below the upper-elevation regions of near continuous bedrock. Auger transects extended upslope from the valley bottom, crossing bedrock outcrops, boulders, and soil-mantled swaths.

Measuring chemical weathering intensity in soils requires quantifying the soil geochemistry and comparing to an associated parent material. Functionally, this is not straightforward in systems with variable grain sizes or course rock fragments. Traditionally, soil chemical analyses focus on the <2 mm fine-earth fraction (Schoeneberger et al., 2012). Though it is recognized that the coarse fraction is important to account for soil geochemistry and geomorphology (Egli et al., 2014), sampling designs across studies are widely variable and typically biased to whatever can be sampled easily. In our sampling design, we consider soil to be all material less than 5 cm in diameter (following Dixon et al., 2012). Coarser surface material and rock exposures are classified either as rock fragments, boulders, or in-place bedrock.

We established a 3 × 3 m grid at 56 sites where we collected soil samples within 9 grid squares (each 1 m^2; Fig. 2). We sampled the top 10 cm of soil within each of the 9 grid-squares and amalgamated these to a single sample to best capture the average soil composition (e.g., Ferrier et al., 2012). We follow Dixon et al. (2009a) by sampling bulk soils for elemental analyses, and do not sieve out coarse fractions >2 mm. We deliberately include material up to 5 cm diameter to more accurately characterize weathering in rocky soils with variable sizes.

Approximately 5–10 rock samples from nearby exposed rock and boulders were collected from the surface within 10 m of the soil grid to represent an average parent material. We aimed to sample rock exposures that were primarily intact, though these were limited in most sample sites, and thus we included samples from detached boulders potentially transported some distance from upslope. Our sample design assumes that the chemical composition of bedrock and rock fragments at the surface is reflective of the parent material from which surface soils were formed. This assumption likely biases our rock samples to those more resistant to weathering, especially at Rye Creek where the weathered soil cover is largely continuous. Despite this drawback in our methods, we have taken steps to improve accuracy over methods that rely on a single rock source or type and that assume soils are only formed from rock directly underlying. Our existing amalgamated rock samples likely reflect to some degree both local and upslope parent materials. By

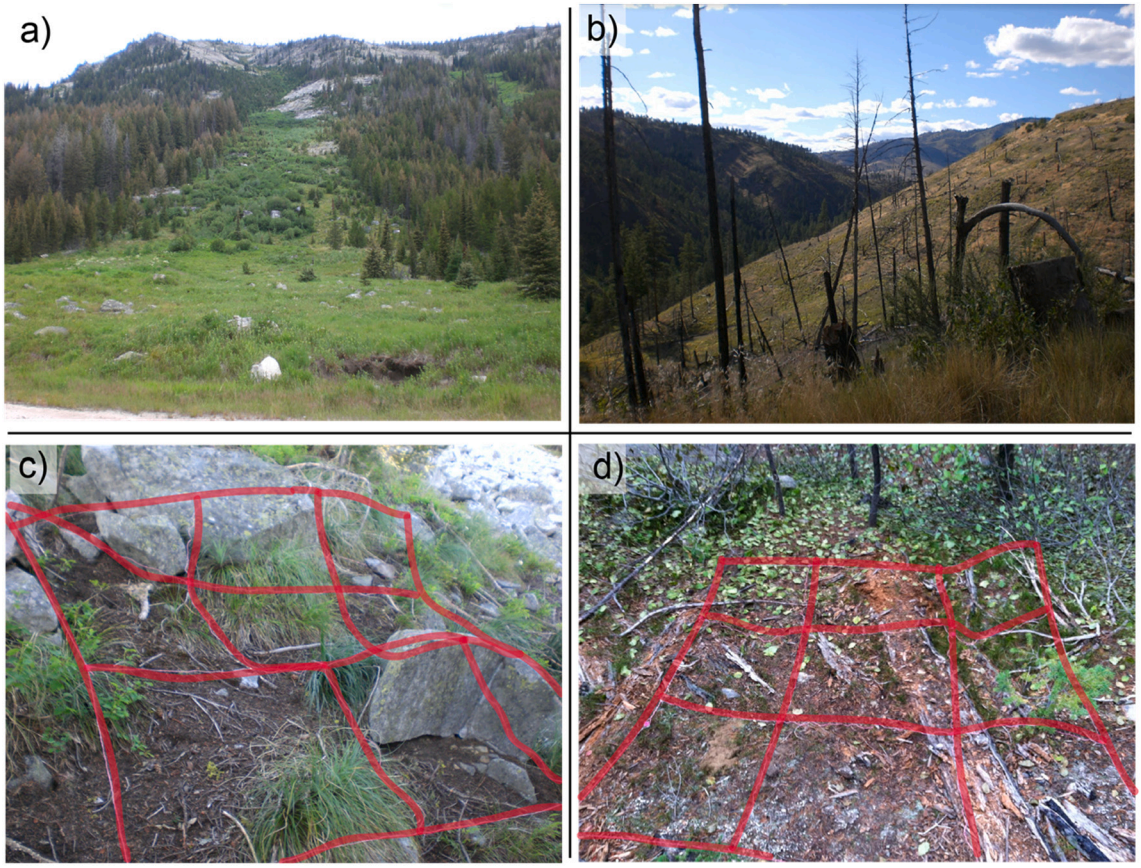

Fig. 2. We quantify soil cover at both the local and landscape scales in Lost Horse (a) and Rye Creek (b). A string grid, outlined in red for visibility, consisting of nine 1 m^2 segments (c, d) was used to estimate local soil and rock cover at each sample location in the field. (For interpretation of the references to color in this figure legend, the reader is referred to the web version of this article.)

amalgamating rock fragments from several rocks rather than a single sample, we minimize the effect that one anomalous sample or exposure might have on our estimate of parent material composition. To further prevent sampling bias, all collected rock samples were crushed to <1 cm and powdered before subsampling for XRF analysis.

Surface regolith cover in these mountain environments included coarse rock fragments >5 cm and sometimes was disrupted by the local exposure of bedrock at the surface. These larger rock fragments and cobbles were not collected and homogenized in soil sampling. To complement auger measurements made of soil and rock cover, we determined the local and finer-resolution extent of rock cover using a grid-based method. The fractional cover of exposed bedrock and rock fragments (>5 cm in length) was estimated within each of the 9 grid segments and averaged to calculate the fractional local exposure of bedrock and effective soil cover at each sample location. We then calculated an effective soil thickness by multiplying the average measured soil thicknesses by the fraction of soil cover. This analysis assumed that the amount of rock exposed at the surface is reflective of rock fragments distributed throughout the soil column (Simanton et al., 1994). We dug six soil pits to compare the depth distribution of rock fragments and validate that surface exposure reflects variability at depth.

3.2. Topographic and land cover analyses

We characterized topography using USGS National Elevation Dataset ~10 m digital elevation models (DEMs; N-S spacing). Though higher-resolution topographic data are available for some valley bottoms and other isolated portions of the study region, those datasets have insufficient coverage for our sample locations and catchment-wide analyses. Terrain attributes, stream networks, and catchment extents were extracted using Spatial Analyst tools in ArcGIS and TauDEM toolset (Tarboton, 1997), and processed in MATLAB software to derive topographic statistics.

In Lost Horse Creek, field measurements of rock exposure were largely limited to lower slopes, primarily below treeline. These rock-cover field measurements from augers and soil-grids are thus detailed and accurate only within the predominantly soil-mantled domain in which they were taken. Areas of more continuous rock exposure were visible from valley floors; these rocky areas tend to be found in high-elevation, very steep, less-accessible settings (Figs. 2a, 3a). In order to identify bedrock exposure in inaccessible regions and at a larger catchment scale, we use a combination of Google Earth Images, ImageJ spectral analysis, and the 2011 National Landcover Database. We selected multiple 100 × 100 m sites at each catchment to explore the applicability of expanded rock and landcover mapping. Using Google Earth, we hand-digitized exposures of rock in 10 selected patches of Lost Horse Creek (Fig. 3). Plots were chosen to span a variety of aspect and slope positions and aimed at rock-soil transitions. In this analysis, we included talus boulder fields in the rock domain. We included 6 validation sites in Rye for consistency, a lower number because the catchment exhibits a near-continuous soil mantle, and rock outcrops are isolated and difficult to identify in aerial imagery due to their small size.

First, we used the 2011 National Land Cover Database (NLCD) dataset (Homer et al., 2015) created by the Multi-Resolution Land Characteristics (MRLC) Consortium, which characterizes land cover at 30 m resolution based primarily on a decision-tree classification of c. 2011 Landsat satellite data. NLCD thematic classes primarily focus on vegetation communities and land use, and as such this database is not aimed at distinguishing rock cover. Here, we use NLCD data because of their wide availability and accessibility to users, and we explore the

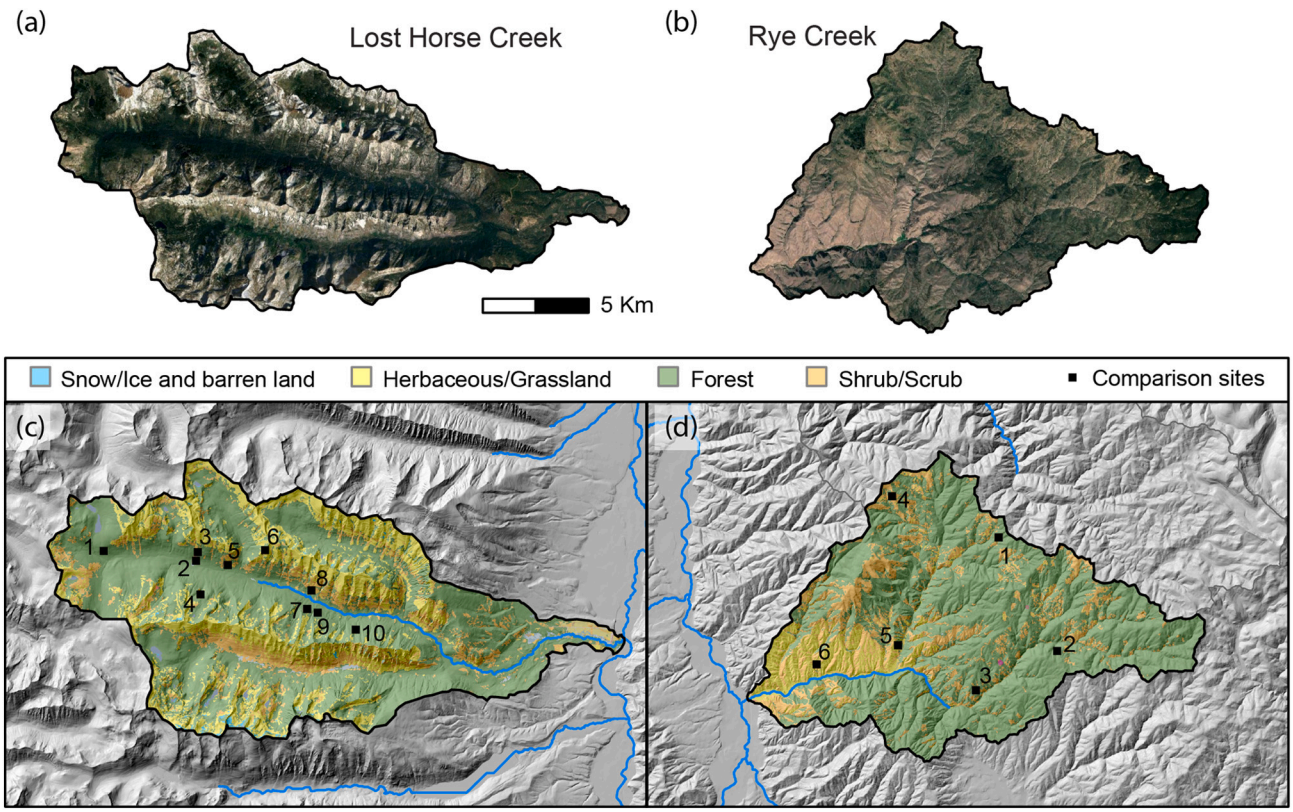

Fig. 3. Google Earth aerial imagery (a, b) and NLCD 2011 land-cover classifications (c, d) were used to map catchment-scale bedrock cover in our study area. Extensive high-elevation bedrock exposures visible in the image of Lost Horse Creek (a) are poorly represented by the "Barren Land (Rock/Sand/Clay)" NLCD category, which makes up less than 0.2% of the mapped catchment (primarily as isolated pixels too small to be visible in panel c). Instead, rock exposures above treeline at Lost Horse overlap with the Herbaceous/Grassland NLCD category, though this category underestimates exposures on north-facing slopes. In Rye Creek (b, d) soil cover is nearly continuous. Multiple 100 × 100 m^2 patches (6 in Rye Creek, 10 in Lost Horse Creek) were selected for detailed bedrock mapping to reclassify NLCD categories and calibrate ImageJ processing.

degree to which reclassified categories serve as proxies of mapped bedrock outcrops. In Lost Horse Creek, the NLCD "Barren Land (Rock/Sand/Clay)" category occupies only 0.2% of the catchment area, far underestimating the rock cover visible in this system (Fig. 3). NLCD categories were compared to bedrock exposures mapped in Google Earth validation plots and field-based ground truthing where possible, in order to reclassify NLCD data into two binary categories: soil and rock. This method allows us to identify and quantify exposed rock quickly across the entire study area rather than exhaustive mapping by hand at a large scale. Workers who intend to explore this method in the future must readjust their classifications for their particular setting of interest.

We also test the use of simple spectral analysis of aerial photography to estimate the proportion of soil and rock cover using ImageJ, a public-domain image-processing program. Due to lack of extensive exposures of bedrock in Rye Creek, where bedrock outcrops tend to occur at a meter-scale, we apply this reclassification at Lost Horse Creek only. Our ImageJ analysis of Google Earth images is based on a simple algorithm that quantifies pixels in an image above a brightness threshold chosen by the user. In this analysis, rock cover was delineated in the 10 Lost Horse Creek validation plots based on brightness of a greyscale aerial image (Fig. 4 and supplementary material). We then applied this threshold to an image of the entire catchment in order to calculate landscape-scale rock and soil cover and compare to the NLCD-based estimates.

3.3. Analysis of chemical weathering extent

We combine the field analysis and the remotely sensed landcover characterization described in the previous two sections to improve our understanding of chemical weathering at multiple spatial scales. Chemical depletion fraction (CDF) and mass transfer coefficients (tau) are well-established metrics of chemical weathering extent (Brimhall and Dietrich, 1987; Riebe et al., 2001). We build on these by adjusting the calculations first to incorporate rock within the soil-mantled domains as measured by our sample grids, and second to incorporate rocky domains using landcover classifications.

We analyzed the bulk elemental composition of 118 soil and rock surface samples by X-ray fluorescence (XRF) spectrometry, performed by ALS Global in Reno, NV.

Bulk samples were completely pulverized to <75 μm. Concentrations of trace elements such as zirconium were measured by pressed-pellet wavelength dispersive XRF. Major oxides were measured on a fused disk of sample mixed with a lithium borate flux. Molar concentrations were calculated from oxide percentages and all concentrations were ash-corrected based on loss on ignition percentages.

We quantify the degree of chemical weathering based on bulk and trace elemental concentrations in soils and bedrock. The chemical depletion fraction (CDF; Riebe et al., 2001, 2003) reflects the relative enrichment of an inert element in soils (i_{soil}) compared to parent material (i_{rock}):

$$CDF = 1 - \left(\frac{i_{rock}}{i_{soil}}\right). \quad (1)$$

Relative losses of major elements (j; Na, Mg, K, Ca) were indexed by mass transfer coefficients (tau; τ_j) (Muir and Logan, 1982; Brimhall and Dietrich, 1987):

$$\tau_j = \frac{j_{soil} * i_{rock}}{j_{rock} * i_{soil}} - 1. \quad (2)$$

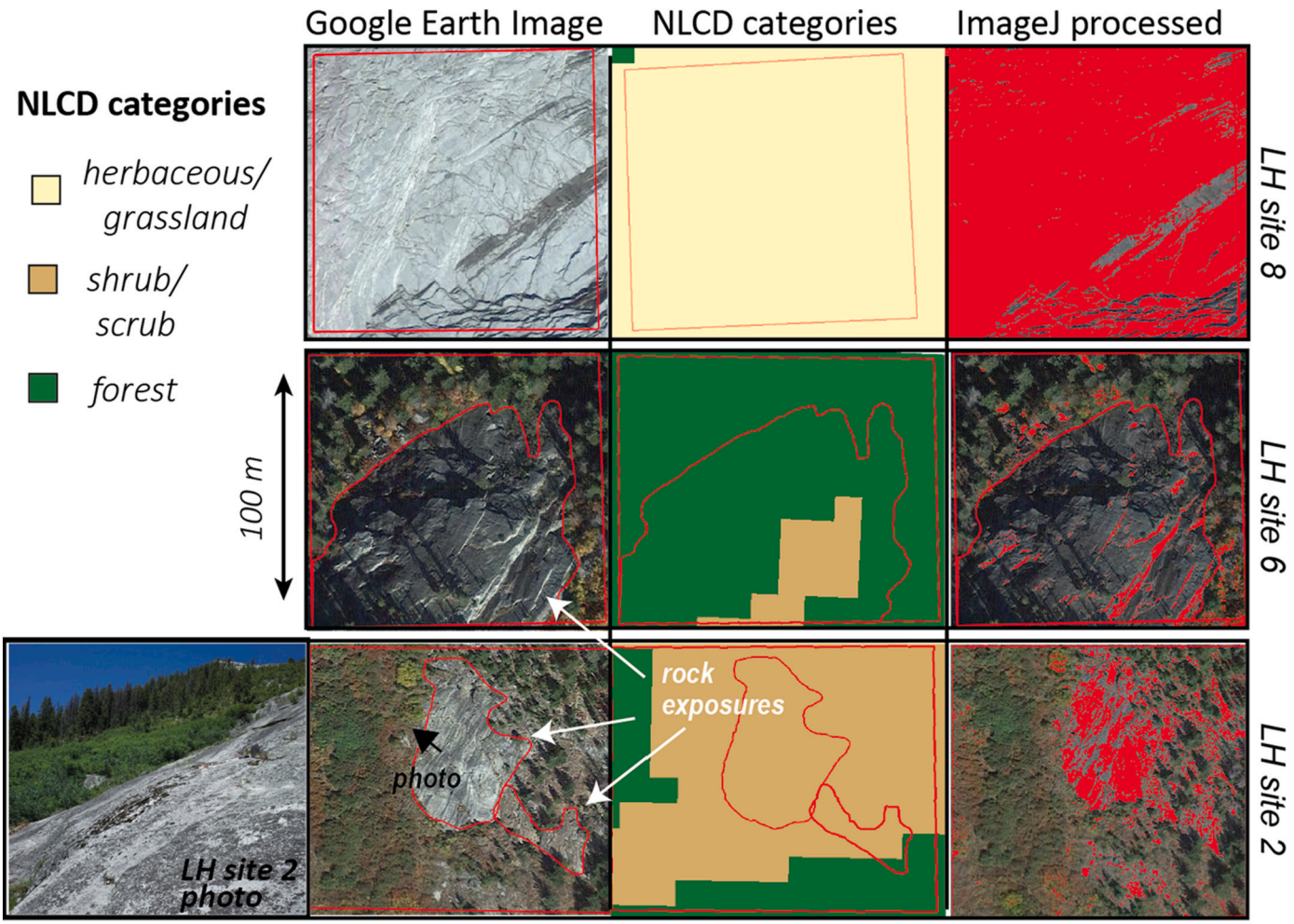

Fig. 4. Subset of selected sites in Lost Horse Creek for comparison of mapped bedrock, NLCD-classifications, and ImageJ spectral processing. Each separate row compares mapped bedrock exposure in the sites with corresponding NLCD categories (middle column) and Image-J analysis (right column). The photograph at the bottom left panel was taken from the ground at the point and perspective of the black arrow for LH site 2. Rock exposures visible in Google Earth are outlined in red. While large expanses of exposed bedrock at Lost Horse Creek were identified well by "grassland/herbaceous" NLCD classes, sites with patchy bedrock (red outlines) were generally found to match multiple NLCD classes (LH site 8). Site locations with the Lost Horse Creek basin are shown in Fig. 3c. In Rye Creek, rock cover was rare and too sparse to correlate with coarse NLCD classes (see supplementary material). (For interpretation of the references to color in this figure legend, the reader is referred to the web version of this article.)

Values of $\tau > 0$ represent fractional mass gain in soil relative to its parent material and $\tau < 0$ represent fractional mass loss. In this analysis we assume 1) soils are derived from bedrock and that inputs from dust sources are negligible; 2) boulders on the surface have similar composition to local and upslope bedrock at depth; and 3) rock and soil contain an immobile element (*i*) that is effectively inert to chemical weathering reactions.

We compared Zr and Ti in soils and rock (Fig. 5) to test that their concentrations varied with little change in ratios, an observation consistent with enrichment during weathering (e.g., Dixon et al., 2012). Eqs. (1) and (2) were applied to soil-rock pairs from each sample site. However, several sites within Rye Creek had anomalous Ti and Zr concentrations relative to their local rock pairs or regional counterparts, likely reflecting inconsistent composition of locally outcropping boulders compared to buried parent material (Fig. 5a). For soil samples paired to these bedrock outliers, weathering indices were calculated using a composite parent material value measured as the average values of all unflagged Rye rock samples. Although this is an inconsistency for these few samples, we find it valuable to keep sample pairs together when possible and do not use a single landscape-averaged rock chemistry value for all sample calculations. The paired rock samples already represent an amalgamation of nearby parent-material sources, and regional rock compositions across the batholith are variable (Fig. 5a).

We use Zr-based CDF and tau values in the remainder of the manuscript consistent with similar studies (e.g., Dixon et al., 2012). The Zr-based values yield lower and more reasonable CDF values than Ti-based measurements, and past studies have suggested Ti-mobility in granitic rocks is higher than that of Zr (Taboada et al., 2006).

We adapt the weathering calculations above (Eqs. (1) and (2)) to develop a new metric accounting for rock fragments within soil-mantled portions of the landscape. Mass transfer coefficients of specific elements and CDF values were multiplied by the grid-based percent soil cover estimate at each sample site to calculate a "rock-adjusted tau" (RAτ) and "rock-adjusted CDF" (RACDF) value. The hyper-local focus of traditional approaches does not account for parent material from rock fragments and bedrock exposed within just a shovel or arm's length. This rock-adjusted value provides an improved characterization of the weathering intensity underfoot at each sample site.

We extend our calculations to a regional scale and adjust CDF and tau values to include the rocky uplands where we assume weathering intensities are minimal compared to regolith values. Using estimates of rock cover based on the landcover analyses described in Section 3.2, we calculate "landscape-adjusted" CDF and tau values as the product of rock-adjusted weathering (RACDF and RAτ) and fractional soil cover (i.

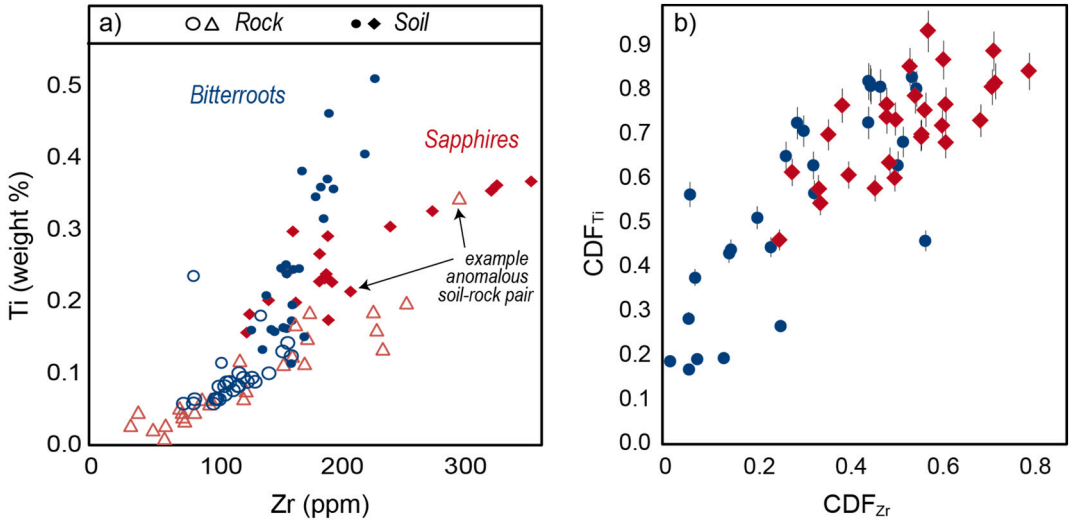

Fig. 5. a) Ti and Zr concentrations of soil (closed symbols) and rock (open symbols) samples. The arrows highlight an example anomalous rock sample where Ti and Zr concentrations exceed the associated soil values. b) CDF values calculated with either Ti (CDF_{Ti}) or Zr (CDF_{Zr}) as refractory elements are correlated, though not a 1:1 relationship. Symbol size exceeds uncertainty unless shown.

e., the proportion of the catchment estimated by NLCD to be mantled by soil). We apply this adjustment to Lost Horse Creek only because Rye Creek lacks significant amounts of exposed and mappable rock.

4. Results

4.1. Topographic variability across study catchments

Slope analysis of catchments within our study region highlights differences between the formerly glaciated Bitterroot Mountains and primarily nonglaciated Sapphire Mountains (Fig. 6). Catchments exhibit similar morphologies within each separate range. Slope gradients of Sapphire catchments are normally distributed about mean slopes of 20.9° ± 0.01 (μ ± s.e.). By contrast, slope gradients of the Bitterroot catchments are higher, averaging 27.5° ± 0.01, with over half of slopes >33°. The focused study catchments, Rye and Lost Horse Creeks, are generally representative of the broader mountain ranges; Lost Horse has a higher mean elevation (2014 m) than Rye (1734 m).

4.2. Soil cover and thickness

Auger-based estimates of soil and regolith cover are highly variable across both Lost Horse and Rye Creek catchments (Fig. 7a, b). Measured soil thicknesses (determined by the absence of relict rock fabric in samples) are less than the augered depths of refusal in Rye Creek. Thus, regolith in this system is composed of both mobile soil and saprolite (Fig. 7a). In comparison, nearly all soils directly mantle rock in Lost Horse Creek, with no saprolite layer. Soils tend to thin with increasing slope at Lost Horse Creek but exhibit little consistent variation with slope at Rye (Fig. 7c, d). Soils are on average two times thicker in Rye Creek (34.9 ± 1.4 cm, $n = 165$) than Lost Horse Creek (17.5 ± 1.5 cm, n = 165; $p < 0.01$). Only 78% of auger sites (146 of 187) within the primarily soil-mantled portions of Lost Horse Creek had measurable soil (>1 cm). We augured 4 points within a 1 m^2 area at two calibration sites in Rye Creek and two in Lost Horse Creek, and found local coefficients of variation of 15% and 27% in Rye and Lost Horse respectively, based on standard deviations of soil thickness.

At a subset of sample sites with soil at the surface, we performed local grid-based measurements of emergent boulders and rock fragments >5

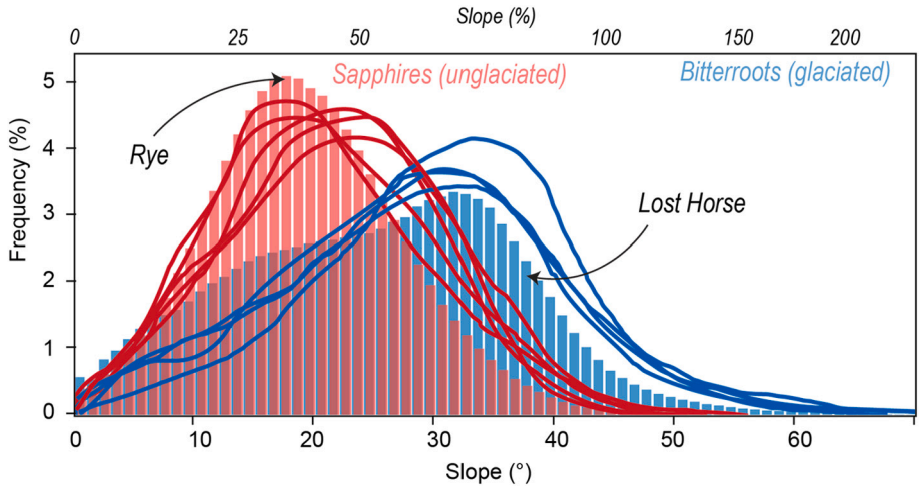

Fig. 6. Slope distributions of 11 catchments in the Bitterroots (blue) and Sapphires (red). The red and blue shaded histograms represent Rye Creek and Lost Horse Creek respectively. Slope distributions generally group by mountain range, with higher modal slopes in the Bitterroots. (For interpretation of the references to color in this figure legend, the reader is referred to the web version of this article.)

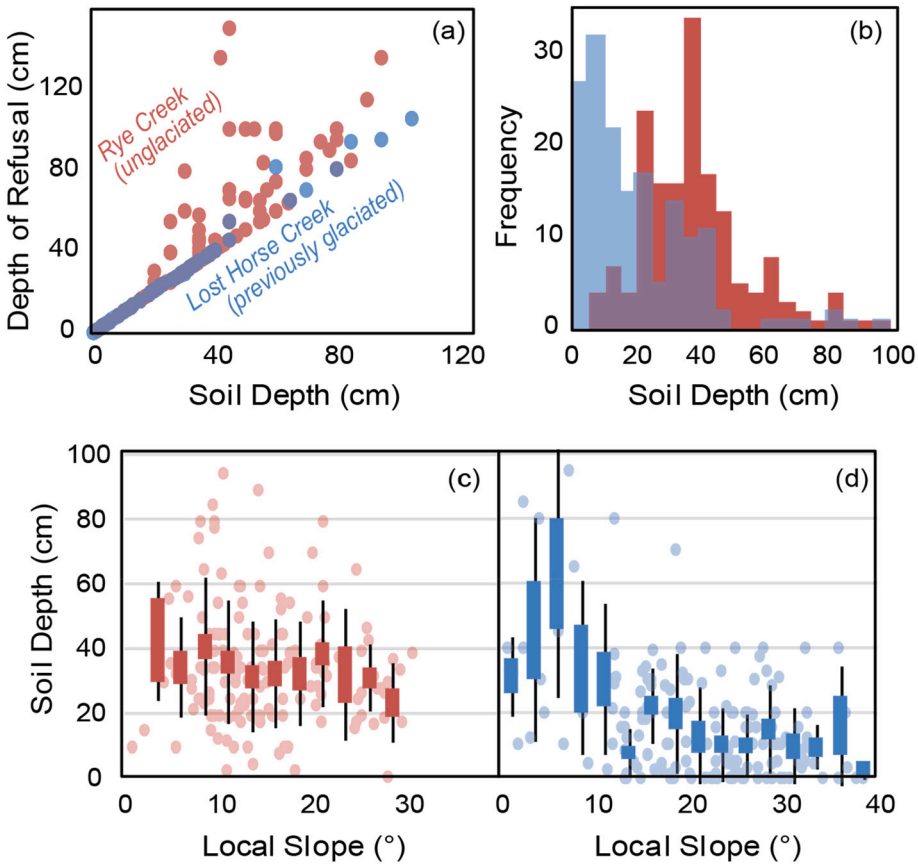

Fig. 7. a) Thin soils (<20 cm) are generally found directly atop bedrock, while greater depths of auger refusal under thicker soils indicate layers of weathered rock (saprolite). b) Soil thicknesses are highly variable across both Rye (red) and Lost Horse (blue) catchments at both local and regional scales, but are generally thicker in the continuously soil mantled region compared to thinner local patches in Lost Horse Creek. We also find distinct relationships between depth and slope gradient (c, d) in these systems. Generally, soils show no clear relationship with slope angle in the continuously soil-mantled Rye Creek system (c), while steep slopes in rockier Lost Horse Creek have thin soils. (For interpretation of the references to color in this figure legend, the reader is referred to the web version of this article.)

cm. Soil cover estimates at Lost Horse and Rye Creek were 86.8% (±2.6%, $n = 23$) and 96.9% (±2.1%, n = 23) respectively. Accounting for auger sites lacking soil in the otherwise primarily-soil-mantled domain of Lost Horse Creek (22%; not included in the above string-grid measurements), the surface soil cover estimate adjusts to 67.7% (Table 1). Thus, within this soil-mantled domain, local rock outcrops and large rock fragments (>5 cm) make up >27.4% of the surface in Lost Horse Creek and 3.1% of the surface in Rye Creek.

Next, we multiply average soil thicknesses (measured by auger) and soil cover estimates (estimated using 3 × 3 m grid at sample sites) to calculate what we term the effective soil thickness. This metric accounts for the observation that even in the largely soil-mantled valley bottom and lower hillslopes of Lost Horse Creek, rock cover influences the ecologic, hydrologic, and geomorphic role of soils. Effective soil thickness in Rye is more than double that of Lost Horse (Table 1; 33.8 cm and 12.7 cm, respectively). Because this comparison only applies to predominantly soil-mantled portions of each landscape and excludes rocky ridges and upper hillslopes of Lost Horse Creek, catchment-scale differences in soil thickness and cover between these two catchments are much greater.

We now broaden our scope to include rocky portions of Lost Horse Creek, those steep uplands where soil is patchy if present at all. This same larger-scale analysis is not relevant in Rye Creek, which lacks steep, rocky areas. While small exposures of rock cover could be mapped in Rye Creek via aerial photography, these were too isolated and small-scale to compare to coarse NLCD landcover classifications (Fig. 3). Nine NLCD landcover classes are found in Lost Horse, and the NLCD "Barren Land (Rock/Sand/Clay)" category occupies only 0.2% of the catchment area, far underestimating rock cover in this system. The coarse resolution and sub-pixel landcover mixing of NLCD data are known to result in underestimations and limited accuracy of mapped extents of "Barren Land" in steep mountain terrain. In the Sierra Nevada Mountains of

Table 1
Chemical weathering intensity and soil thickness.

	Lost horse (bitterroots)			Rye (sapphires)		
	Avg	±Std err	n	Avg	±Std err	n
Element-specific tau[a]						
τ Si	−0.30	±0.04	28	−0.55	±0.03	28
τ Al	−0.26	±0.03	28	−0.43	±0.05	28
τ Na	−0.42	±0.04	28	−0.55	±0.04	28
τ K	−0.39	±0.04	28	−0.65	±0.03	28
Rock-adjusted tau[b]						
RA τ Si	−0.22	±0.05	23	−0.53	±0.05	27
RA τ Al	−0.19	±0.05	23	−0.42	±0.06	27
RA τ Na	−0.30	±0.05	23	−0.53	±0.06	27
RA τ K	−0.28	±0.06	23	−0.63	±0.06	27
Soil cover and thickness						
Auger refusal depth (cm)[c]	18.2	±1.6	164	41.1	±2.1	165
Soil thickness (cm)	17.5	±1.5	163	34.9	±1.4	165
Local soil cover (%)	67.7			96.9		
Effective soil thickness (cm * %area)[b]	12.7			33.8		
Soil and surface weathering						
CDF	0.29	±0.03	28	0.53	±0.03	28
RACDF[b]	0.20			0.51		
Landscape-adjusted RACDF[d]	0.14			0.51		

[a] Negative tau (τ) values reflect element-specific weathering loss.
[b] Rock-adjusted weathering (RA-τ, RACDF) and effective soil thickness incorporate local-scale rock fractions, based on string grids at sample sites.
[c] Auger refusal depth differs from soil thickness when saprolite is present.
[d] Landscape-adjusted RACDF is the average RACDF times landscape-scale soil-cover and is therefore the most comprehensive measure of landscape-wide chemical weathering we produce.

California, NLCD categories underestimate rock at high-gradient slopes (similar to the high-elevation cliffs of our study area) up to 88% (Petliak et al., 2019). Visual comparison with aerial photography (Fig. 3) identified three categories ("Perennial Ice/Snow," "Barren Land (Rock/Sand/Clay)," and "Grassland/Herbaceous") that best match mapped rock cover at both a catchment scale (Fig. 3) and across the rock-soil transitions seen in Lost Horse Creek validation plots (Fig. 4). Predominantly soil-mantled slopes coincide with the other classifications, including "Evergreen Forest", "Woody Wetlands", "Emergent Herbaceous Wetlands", and "Pasture/Hay". The "Shrub/Scrub" category, which makes up 12% of total area of Lost Horse Creek, often occurred at the edges of clear bedrock regions and included significant rock outcrops (Fig. 3). In our conservative metric of rock cover, erring on the side of underestimating rock exposure (and thus underestimating the weathering differences between soil-mantled versus steep terrain), we classified "Shrub/Scrub" as soil. This results in an NLCD-based estimate of rock cover in Lost Horse Creek catchment of 28.6%.

Iterative ImageJ analysis of aerial imagery in 10 validation plots (Fig. 3) was used to visually determine a brightness threshold of 135 (on an 8-bit greyscale, where 0 = black and 255 = white) that delineated rock and soil portions of the landscape. We selected a threshold that conservatively identified mapped soil swaths in the validation plots. Thus, these methods likely provide a slight underestimation of rock exposure. Applying this threshold across the entire catchment, we find that at least 29.6% of Lost Horse Creek has exposed bedrock.

Applied at the landscape scale, both NLCD and ImageJ analysis of aerial imagery indicate just under one third of land surface area in Lost Horse Creek has exposed bedrock at the surface (Fig. 8; 28.6% by NLCD; 29.6% by ImageJ). Our visual comparison does not provide a robust test of NLCD- and Google Earth-based analyses of landscape rock cover, which is beyond the scope of this study. However, their agreement suggests both are reasonable (though conservative) estimates.

Our catchment-scale methods map similar areas of bedrock cover (Fig. 8), though there is some disagreement at a fine scale. While both methods are effective at capturing extensive rocky ridges, we find disagreement mostly 1) at the transition between hillslopes and ridges, where vegetative cover is patchy and coarse NLCD resolution is limiting, 2) on soil-mantled avalanche chutes that have high brightness in ImageJ analysis, and 3) along shadowed rocky ridges and scree slopes that ImageJ analysis misidentifies as soil. We adopt the rock cover estimate from NLCD reclassification (28.6%) for the following calculations.

4.3. Chemical weathering intensity

First, chemical depletion fractions (CDF) calculated from zirconium concentrations in soils and bedrock, on average indicate local soils at Lost Horse Creek are 45% less weathered than those at Rye Creek (0.29 ± 0.03, $n = 27$ and 0.53 ± 0.03, $n = 28$ respectively; $p < 0.01$). Mass transfer coefficients (τ) of major elements (Si, Na, and K) also tend to be higher in Rye (Table 1; using two-sample *t*-tests assuming unequal variances, τSi and τK significant at $p < 0.01$; τNa $p = 0.03$). Notably, τNa, which is often used as an indicator of plagioclase weathering (e.g., Rasmussen et al., 2011) is highly variable in both systems and ranges from −0.10 to −0.68 in Lost Horse Creek and from 0.03 to −0.83 in Rye Creek, averaging −0.43 ± 0.17 ($n = 27$) and −0.53 ± 0.23 ($n = 28$) respectively.

CDF measurements range surprisingly high (Fig. 10). Though we do not know the fraction of quartz in regional bedrock, estimates of weathering intensities upwards of 70% are likely impractical. These high values may result from a sampling design reliant on bedrock exposures that are of a different composition than buried bedrock and are more resistant to weathering. Regardless, we have attempted to improve sampling methods over past studies that are heavily reliant on single bedrock samples, and CDF values should provide a valid, if relative, measure of weathering intensity for landscapes with a patchy soil mantle.

Local Rock-Adjusted CDF values (RACDF) and element-specific losses (RAτ) incorporate an adjustment for rock-fragments and bedrock exposure within sampled soil-mantled areas (i.e. valley bottoms and lower hillslopes) based on our field sampling grids. These metrics provide a more accurate picture of the profound differences in catchment-scale weathering intensity and soil formation between Rye and Lost Horse. RACDF values average ~41% higher in Rye Creek compared to Lost Horse (0.51 and 0.20 respectively; $p < 0.01$). Elemental differences (RAτ of Si, Na, and K) between soils in Lost Horse Creek also become magnified by rock adjustment, while rock adjustment in Rye Creek does not change the numbers significantly (Table 1).

Finally, we widen our scope to include the highest and steepest portions of Lost Horse Creek where bedrock is exposed. Multiplying the percent of Lost Horse's total area that is mantled by soil (71.4%) by its RACDF (0.2) we calculate Lost Horse's landscape-adjusted CDF to be 0.14 (Table 1). We offer this as the most comprehensive estimate of chemical weathering intensity across the entire catchment.

5. Discussion

Detailed analysis of two study catchments, Lost Horse and Rye Creek, showed differences in soil cover and thickness at local and landscape scales. Within the >70% of Lost Horse catchment that is soil-mantled (Fig. 9), local rock outcrops and large rock fragments make up a significant portion (27%) of the surface (Table 1; Fig. 2). Bedrock dominance increases and soil thicknesses decrease with increasing slope gradients in Lost Horse Creek both locally (Fig. 5) and at a landscape scale (Fig. 9). Thus, we find no clear critical slope thresholds above which soil does not persist, similar to past studies, although thresholds may emerge when viewed at finer resolutions (e.g., DiBiase et al., 2012). An apparent decrease in rock cover at gradients >40° is likely due to the poor applicability of NLCD as a proxy at these steep slopes (Petliak et al.,

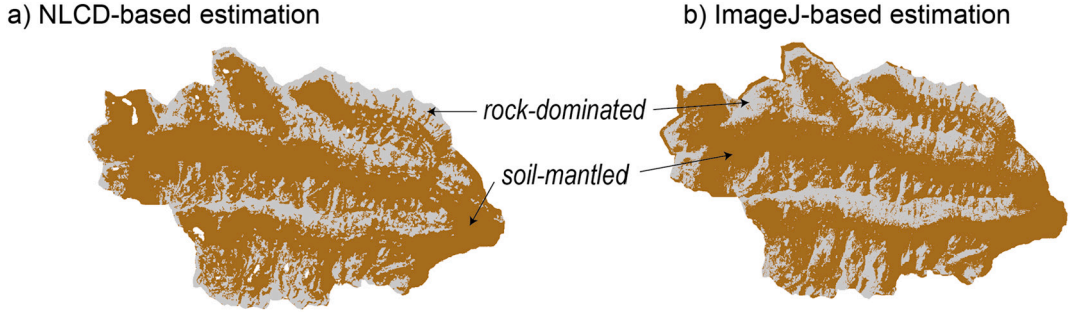

Fig. 8. Comparison of rocky (grey) and soil-mantled (brown) regions within Lost Horse Creek based on two methods, (a) NLCD vegetation reclassifications and (b) spectral image classification of aerial photography using Image-J analysis software. Both methods yield a similar estimate of ~30% rock cover in this catchment. (For interpretation of the references to color in this figure legend, the reader is referred to the web version of this article.)

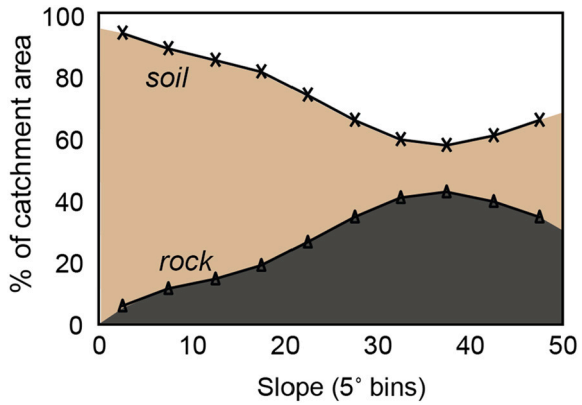

Fig. 9. NLCD-derived rock and soil categories versus slope (binned by 5° increments) within the Lost Horse catchment. In total, our NLCD-derived rock category composes ~30% of the land cover in Lost Horse. Rock cover increases noticeably with slope gradient, from only 6% rock cover at slopes <5° to ~40% at slopes >35°. The apparent decrease in rock cover at the highest slopes is likely due to the low-resolution of NLCD data and poor accuracy in rocky and steep terrain (Petliak et al., 2019).

2019), which occur intermittently along thin bands of the Lost Horse catchment. Importantly, soils are present in roughly half the landscape even at steepest slope angles (Fig. 9). While increases in slope gradients do not result in an observable threshold response in soil cover and abundance, they correlate with a gradual doubling in rock cover at a landscape scale, and thus we infer important process changes that co-vary with slope.

Weathering indices consistently show that sampled soils in the unglaciated Rye Creek are more highly weathered than post-glacial Lost Horse Creek. CDF and τ values of major elements derived from weatherable minerals (Si, Na, and K) indicate nearly double the weathering intensity at soils in Rye Creek watershed compared to soil-mantled portions of Lost Horse. This difference could arise if soils are 'older' in Rye Creek due to the lack of glaciation. Based on denudation rates at similar settings around the globe (Portenga and Bierman, 2011), the relatively thin soils (<50 cm), and the time since glacial retreat, we suspect that soil residence times may be similar in the two catchments. Instead, we anticipate that the lack of glacial erosion in Rye allowed the bedrock weathering front to outpace soil production long term (as evidenced in the observed saprolites in Rye; Fig. 7a) and thus soils are derived from pre-weathered parent material (saprolite).

On average, Na and K losses are high in both systems and suggest strong weathering of plagioclase and potassium feldspar. These similarities are not surprising based on the uniform lithology across the catchments, and the expectation that feldspar dissolution dominates weathering losses in granitic catchments (Rasmussen et al., 2011).

These soil-based indices underestimate differences in surface weathering because they include locations with significant rock exposure and rock fragment contributions to soils. Adjustments for unweathered rock contributions in the near surface (e.g., calculation of RACDF) reduce measured chemical intensities from 29% to ~20% in Lost Horse Creek and from 53% to 51% in Rye Creek. Accounting for landscape-scale rock emergence further reduces estimates of chemical weathering intensity in Lost Horse Creek to 14%. This derivation assumes areas of exposed bedrock undergo trivial weathering. It also requires accurate quantification of soil-mantled and rocky portions of the landscape. Our study is limited by the exclusion of weathering in deep fractures and the facets of talus fragments. However, even with significant error, the approximations presented here should more accurately reflect landscape weathering differences between the two catchments than is captured by soil geochemistry results alone.

Most studies based on regolith data focus solely on kinetic- and supply-limited regimes focused in landscapes with a continuous soil

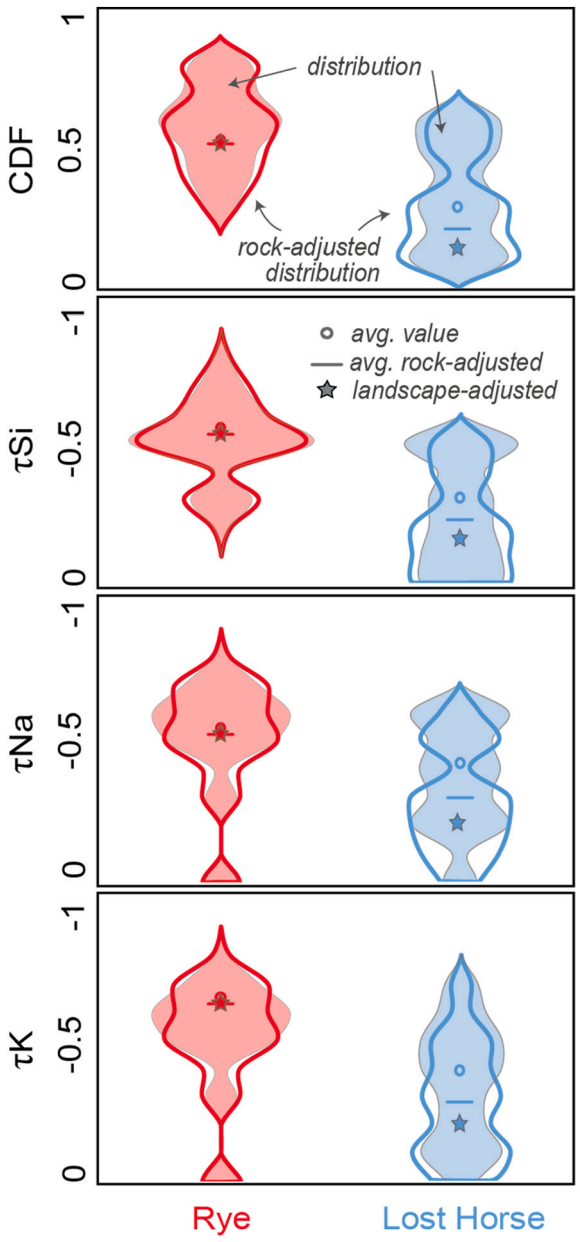

Fig. 10. Weathering indices for soils in Rye (red) and Lost Horse (blue) catchments. Raw data distribution of soil CDF and element specific losses are shown as shaded violin plots. The distribution of rock-adjusted weathering indices (RACDF and RAτ) is represented by hollow violins, and is calculated by multiplying individual sample CDF and τ-values by the percent soil cover estimated at that sample site using a 3 × 3 m string grid (Fig. 2). Average values of CDF and τ are shown by circles, while the rock-adjusted mean is represented by a horizontal line. Landscape-scale surface weathering intensity (accounting for large-scale rock cover within study systems) is represented by the star. Because NLCD methods were unable to identify sparse, isolated boulders in Rye Creek, landscape-scale weathering averages (star) are the same as the Rock-Adjusted values (line). (For interpretation of the references to color in this figure legend, the reader is referred to the web version of this article.)

mantle (Riebe et al., 2003; Mao et al., 2018) or at a local scale that does not take into account the emergence of rock (e.g., Dixon et al., 2012; Larsen et al., 2014). However, rock cover and abundance, in addition to biasing chemical weathering measurements, also play an important role in local and landscape processes. Rock fragments influence chemical weathering rates (White and Brantley, 2003), and their delivery to channels impacts fluvial sediment dynamics and incision (Sklar et al.,

2017; Shobe et al., 2016; Shobe et al., 2018; DiBiase et al., 2018). Rock cover is also diagnostic of weathering conditions and processes within a system. The consistencies in soil mantle and soil thickness and the high intensity of weathering across Rye Creek suggest a largely supply-limited weathering scenario at both local and landscape scales. By contrast, we find several conditions in Lost Horse Creek that are diagnostic of kinetic-limited weathering (an interpretation that does not require measured erosion rates). First, soils exhibit a wide range of weathering extents, and in some soils a high portion of Na from bedrock remain, an indication that weatherable plagioclase persists. By contrast, in a supply-limited weathering systems one would expect intense and less-variable weathering intensities. Second, local soils directly overlie rock, such that little or no saprolite layer exists beneath mobile regolith. This condition is consistent with the outpacing of a chemical-weathering front by biophysical erosion and soil production (Dixon et al., 2012). Next, soils contain abundant large rock fragments (cobble size or larger) that persist in the weathering reactor. Finally, at a catchment and landscape scale, rock cover is spatially abundant and patchy soils are evident.

We find little correlation between weathering intensity and local topographic metrics (Green et al., 2006; Dixon et al., 2012). This may be attributable to the difference in DEM resolution and the scale of chemical weathering measurements. Our calculations of slope and curvature reflect topographic conditions at a scale of ~900 m^2 (or 9 pixels of a 10 m DEM). This resolution is too coarse to capture the variations in our local soil weathering and rock-adjusted soil weathering measurements (1 m^2 scale) across the landscape. Analysis of high-resolution (~1 m) topography could provide further insight into controls on local soil processes (e.g., DiBiase et al., 2012; Milodowski et al., 2015). Alternatively, we may also infer that highly heterogeneous weathering in our mountainous study landscape reflects a number of complex controls not explicitly quantified here. For example, surface and subsurface hydrology, vegetation and other biotic influences, and fracture-controlled weathering are likely highly variable at a local scale and may overprint other topographic controls. Further complexity may arise if chemical weathering occurs primarily in transient depositional settings such as landslides, rather than in-situ produced soils (Emberson et al., 2016), or as a combination of both. This scenario could result in a decoupling of weathering and the topographic controls we might otherwise expect to influence mineral residence time at the surface.

6. Conclusions

Exploiting two landscapes that present useful contrasts in soil cover and morphology, we provide new data and insights into how weathering, topography, and soil cover relate. We introduce rock-adjusted and landscape-adjusted chemical weathering metrics to refine measurements of chemical weathering intensity in complex settings. We demonstrate that rock cover at local and landscape scales has important implications for calculations of weathering intensity in these systems. In Lost Horse Creek, accounting for abundant rock at local and landscape scales resulted in reductions of calculated landscape-averaged surface weathering intensities by ~50%. These findings suggest that studies that solely rely on fine-regolith chemistry and/or focus only on weathering in hyper-local or isolated soil-mantled portions of the landscape may overestimate weathering regimes and controls in mountainous systems. We suggest adapted chemical weathering metrics, local rock and landscape-adjusted CDF and τ, to address this complexity and resolve biases that result from underestimated rock cover.

Our work also adds new insights into the heterogeneity of critical zone architecture in a complex mountainous landscape. Few studies have quantified spatial variability in soil and bedrock cover (e.g., Norton and Von Blanckenburg, 2010; DiBiase et al., 2012) or rock fragments (Marshall and Sklar, 2012) across mountainous watersheds. We find rock cover (locally emergent bedrock, boulders, and large rock fragments within soils) is ubiquitous at multiple scales, and accounts for a significant component of the surface in the Lost Horse Creek study catchment at both the local and landscape scale. Quantifying bedrock cover and the controls on its emergence will be important in future studies as we seek improved understanding of the chemical and physical processes that release rock-derived nutrients, sculpt and shape mountain systems, and play a critical role in Earth's carbon cycle.

Declaration of competing interest

The authors declare that they have no known competing financial interests or personal relationships that could have appeared to influence the work reported in this paper.

Acknowledgements

We thank Tony Hartshorn and Dave Mogk for their valuable input on the master's thesis from which this manuscript was adapted. We also thank three anonymous reviewers for feedback on an earlier version. This work was supported by the NASA Earth and Space Science Fellowship Program – Grant NNX15AN31H S01 (JLD and SSB), NSF GLD-1644624 (JLD), NSF GLD-1644619 (ACW); NSF EPS-1101342 (JLD) and multiple grants (SSB) from the Montana Water Science Center, the Montana Geological Society, the Montana State University College of Letters and Science, and the Montana Association of Geographic Information Professionals.

Appendix A. Supplementary data

Supplementary data to this article can be found online at https://doi.org/10.1016/j.geomorph.2022.108186.

References

Alden, W.C., 1953. Physiography and glacial geology of western Montana and adjacent areas. In: U.S. Geological Survey Professional Paper, 231, p. 200.
Anderson, R.S., Rajaram, H., Anderson, S.P., 2019. Climate driven coevolution of weathering profiles and hillslope topography generates dramatic differences in critical zone architecture. Hydrol. Process. 33 (1), 4–19.
Anderson, S.P., Dietrich, W.E., Brimhall Jr., G.H., 2002. Weathering profiles, mass-balance analysis, and rates of solute loss: linkages between weathering and erosion in a small, steep catchment. Geol. Soc. Am. Bull. 114, 1143–1158.
Anderson, S.P., von Blanckenburg, F., White, A.F., 2007. Physical and chemical controls on the critical zone. Elements 3 (5), 315–319.
Ben-Asher, M., Haviv, I., Crouvi, O., Roering, J.J., Matmon, A., 2021. The convexity of carbonate hilltops: 36Cl constraints on denudation and chemical weathering rates and implications for hillslope curvature. GSABull. 133 (9–10), 1930–1946. https://doi.org/10.1130/B35658.1.
Berner, R.A., Lasaga, A.C., Garrels, R.M., 1983. The carbonate-silicate geochemical cycle and its effect on atmospheric carbon dioxide over the past 100 million years. Am. J. Sci. 283, 641–683.
Bluth, G.J.S., Kump, L.R., 1994. Lithological and climatological controls of river chemistry. Geochim. Cosmochim. Acta 58, 2341–2359.
Brantley, S.L., Lebedeva, M.I., Balashov, V.N., Singha, K., Sullivan, P.L., Stinchcomb, G., 2017. Toward a conceptual model relating chemical reaction fronts to water flow paths in hills. Geomorphology 277, 100–117.
Brimhall, G.H., Dietrich, W.E., 1987. Constitutive mass balance relations between chemical composition, volume, density, porosity, and strain in metasomatic hydrochemical systems: results on weathering and pedogenesis. Geochim. Cosmochim. Acta 51 (3), 567–587.
Burke, B.C., Heimsath, A.M., Dixon, J.L., Chappell, J., Yoo, K., 2009. Weathering the escarpment: chemical and physical rates and processes, south-eastern Australia. Earth Surf. Process. Landf. 34, 768–785.
Burke, B.C., Heimsath, A.M., White, A.F., 2007. Coupling chemical weathering with soil production across soil-mantled landscapes. Earth Surf. Process. Landf. 32, 853–873.
DiBiase, R.A., Rossi, M.W., Neely, A.B., 2018. Fracture density and grain size controls on the relief structure of bedrock landscapes. Geology 46 (5), 399–402.
DiBiase, R.A., Heimsath, A.M., Whipple, K.X., 2012. Hillslope response to tectonic forcing in threshold landscapes. Earth Surf. Process. Landf. 37 (8), 855–865.
Dixon, J.L., Heimsath, A.M., Amundson, R.C., 2009a. The critical role of climate and saprolite weathering in landscape evolution. Earth Surf. Process. Landf. 34, 1507–1521.
Dixon, J.L., Heimsath, A.M., Kaste, J.M., Amundson, R., 2009b. Climate driven processes of hillslope weathering. Geology 37 (11), 975–978.
Dixon, J.L., Hartshorn, A.S., Heimsath, A.M., DiBiase, R.A., Whipple, K.X., 2012. Chemical weathering response to tectonic forcing: a soils perspective from the San Gabriel Mountains, California. Earth Planet. Sci. Lett. 323, 40–49.

Dixon, J.L., von Blanckenburg, F., 2012. Soils as pacemakers and limiters of global silicate weathering. C.R.Geosci. 344, 597–609.
Dixon, J.L., von Blanckenburg, F., Stuwe, K., Christl, M., 2016. Glaciation's topographic control on Holocene erosion at the eastern edge of the Alps. Earth Surf. Dynam. Discuss. https://doi.org/10.5194/esurf-2016-29.
Edmond, J.M., Palmer, M.R., Measures, C.I., Brown, E.T., Huh, Y., 1996. Fluvial geochemistry of the northeastern Andes and its foredeep in the drainage of the Orinoco in Columbia and Venezuela. Geochim. Cosmochim. Acta 60, 2949–2976.
Egli, M., Dahms, D., Norton, K., 2014. Soil formation rates on silicate parent material in alpine environments: different approaches–different results? Geoderma 213, 320–333.
Emberson, R., Hovius, N., Galy, A., Marc, O., 2016. Chemical weathering in active mountain belts controlled by stochastic bedrock landsliding. Nat. Geosci. 9 (1), 42–45.
Ferrier, K.L., Kirchner, J.W., 2008. Effects of physical erosion on chemical denudation rates: a numerical modeling study of soil-mantled hillslopes. Earth Planet. Sci. Lett. 272, 591–599.
Ferrier, K.L., Kirchner, J.W., Finkel, R.C., 2012. Weak influences of climate and mineral supply rates on chemical erosion rates: Measurements along two altitudinal transects in the Idaho Batholith. J.Geophys.Res.Earth Surf. 117 (F2).
Ferrier, K.L., Riebe, C.S., Hahm, Jesse W., 2016. Testing for supply-limited and kinetic-limited chemical erosion in field measurements of regolith production and chemical depletion. Geochem. Geophys. Geosyst. 17 (6), 2270–2285.
Fletcher, R.C., Buss, H.L., Brantley, S.L., 2006. A spheroidal weathering model coupling porewater chemistry to soil thicknesses during steady-state denudation. Earth Planet. Sci. Lett. 244 (1-2), 444–457.
Foster, D., Brocklehurst, S.H., Gawthorpe, R.L., 2008. Small valley glaciers and the effectiveness of the glacial buzzsaw in the northern Basin and Range, USA. Geomorphology 102, 624–639.
Foster, D.A., Raza, A., 2002. Low-temperature thermochronological record of exhumation of the Bitterroot metamorphic core complex, northern Cordilleran Orogen. Tectonophysics 349 (1–4), 23–36.
Foster, D.A., Schafer, C., Fanning, C.M., Hyndman, D.W., 2001. Relationships between crustal partial melting, plutonism, orogeny, and exhumation: Idaho-Bitterroot batholith. Tectonophysics 342 (3–4), 313–350.
Gabet, E.J., Bookter, A., 2008. A morphometric analysis of gullies scoured by post-fire progressively bulked debris flows in southwest Montana, USA. Geomorphology 96 (3), 298–309.
Gabet, E.J., Mudd, S.M., 2009. A theoretical model coupling chemical weathering rates with denudation rates. Geology 37, 151–154.
Garrels, R.M., Mackenzie, F.T., 1971. Evolution of Sedimentary Rocks. Norton, New York.
Green, E.G., Dietrich, W.E., Banfield, J.F., 2006. Quantification of chemical weathering rates across an actively eroding hillslope. Earth Planet. Sci. Lett. 242, 155–169.
Hahm, W.J., Riebe, C.S., Lukens, C.E., Araki, S., 2014. Bedrock composition regulates mountain ecosystems and landscape evolution. Proc. Natl. Acad. Sci. 111, 3338–3343.
Heimsath, A.M., DiBiase, R.A., Whipple, K.X., 2012. Soil production limits and the transition to bedrock-dominated landscapes. Nat. Geosci. 5, 210–214.
Homer, C.G., Dewitz, J.A., Yang, L., Jin, S., Danielson, P., Xian, G., Coulston, J., Herold, N.D., Wickham, J.D., Megown, K., 2015. Completion of the 2011 National Land Cover Database for the conterminous United States-Representing a decade of land cover change information [dataset] Photogramm. Eng. Remote Sens. 81, 345–354.
Hostetler, S.W., Clark, P.U., 1997. Climatic controls of western U.S. glaciers at the Last Glacial Maximum. Quat. Sci. Rev. 16, 505–511. https://doi.org/10.1016/S0277-3791 (96)00116-3.
Hoffman, D.F., Gabet, E.J., 2007. Effects of sediment pulses on channel morphology in a gravel-bed river. Geol. Soc. Am. Bull. 119 (1–2), 116–125.
Hyde, K.D., Wilcox, A.C., Jencso, K., Woods, S., 2014. Effects of vegetation disturbance by fire on channel initiation thresholds. Geomorphology 214, 84–96.
Hyndman, D.W., 1980. Bitterroot dome-Sapphire tectonic block, an example of a plutonic-core gneiss-dome complex with its detached suprastructure. Geol.Soc.Am. Mem. 153, 427–444.
Kutzbach, J.E., Ruddiman, W.F., 1993. Model description, external forcing, and surface boundary conditions. In: Global Climates Since the Last Glacial Maximum. University of Minnesota Press, pp. 12–23.
Larsen, I.J., Almond, P.C., Eger, A., Stone, J.O., Montgomery, D.R., Malcolm, B., 2014. Rapid soil production and weathering in the Southern Alps, New Zealand. Science 343 (6171), 637–640.
Lebedeva, M.I., Brantley, S.L., 2013. Exploring geochemical controls on weathering and erosion of convex hillslopes: beyond the empirical regolith production function. Earth Surf. Process. Landf. 38 (15), 1793–1807.
Lewis, R.S., 1998. Geologic map of the Montana part of the Missoula West 30′ × 60′ quadrangle: Montana Bureau of Mines Open-File Report 373, scale 1:100,000.
Lonn, J.D., Berg, R.B., 1996. Preliminary geologic map of the Bitterroot Valley, Montana: Montana Bureau of Mines Open-File Report 340, scale 1:100,000.
Lonn, J.D., McDonald, C., Lewis, R.S., Kalakay, T.J., O'Neill, J.M., Berg, R.B., Hargrave, P., 2003. Preliminary Geologic Map of the Philipsburg 30' x 60' Quadrangle, Western Montana: Montana Bureau of Mines Open-File Report 483, Scale 1:100,000.
Maher, K., Chamberlain, C.P., 2014. Hydrologic regulation of chemical weathering and the geologic carbon cycle. Science 343 (6178), 1502–1504.
Mao, H., Zhao, Z., Cui, L., Liu, C., 2018. The influence of climate and topography on chemical weathering of granitic regoliths in the monsoon region of China. Acta Geochim. 37 (5), 758–768.
Marshall, J.A., Sklar, L.S., 2012. Mining soil databases for landscape-scale patterns in the abundance and size distribution of hillslope rock fragments. Earth Surf. Process. Landf. 37, 287–300.
[dataset] MBMG seamless database. Last Queried August 2018. http://mbmg.mtech.edu/gis/gis-server.asp.
Meybeck, M., 1987. Global chemical weathering of surficial rocks estimated from river dissolved loads. Am. J. Sci. 287, 401–428.
Milodowski, D.T., Mudd, S.M., Mitchard, E.T.A., 2015. Topographic roughness as a signature of the emergence of bedrock in eroding landscapes. Earth Surf.Dyn. 3 (4), 483–499.
Mudd, S.M., Yoo, K., Gabet, E.J., 2013. Influence of chemical weathering on hillslope forms. Treat. Geomorphol. 7 (5), 56–65.
Muir, J.W., Logan, J., 1982. Eluvial/illuvial coefficients of major elements and the corresponding losses and gains in three soil profiles. J. Soil Sci. 33.2, 295–308. https://doi.org/10.1002/9781118786352.
Naylor, S., Gabet, E.J., 2007. Valley asymmetry and glacial versus nonglacial erosion in the Bitterroot Range, Montana, USA. Geology 35 (4), 375–378.
Norton, K.P., Von Blanckenburg, F., 2010. Silicate weathering of soil-mantled slopes in an active Alpine landscape. Geochim. Cosmochim. Acta 74 (18), 5243–5258.
Parrett, C., Cannon, S.H., Pierce, K.L., 2004. Wildfire-related floods and debris flows in Montana in 2000 and 2001 (No. 3-4319). In: US Geological Survey.
Pederson, V.K., Egholm, D.L., 2013. Glaciations in response to climate variations preconditioned by evolving topography. Nature 493, 206–210.
Pelletier, J.D., Rasmussen, C., 2009. Quantifying the climatic and tectonic controls on hillslope steepness and erosion rate. Lithosphere 1 (2), 73–80. https://doi.org/10.1130/L3.1.
Perron, J.T., 2017. Climate and the pace of erosional landscape evolution. Annu. Rev. Earth Planet. Sci. 45, 561–591.
Petliak, H., Cerovski-Darriau, C., Zaliva, V., Stock, J., 2019. Where's the Rock: using convolutional neural networks to improve land cover classification. Remote Sens. 11 (19), 2211.
Portenga, E.W., Bierman, P.R., 2011. Understanding Earth's eroding surface with 10Be. GSA-Today 21 (8). https://doi.org/10.1130/G111A.1.
[dataset] PRISM Climate Group. Oregon State University. Last Queried May 2016. http://prism.oregonstate.edu. created 4 Feb 2004.
Rasmussen, C., Brantley, S., Richter, D.D., Blum, A., Dixon, J., White, A.F., 2011. Strong climate and tectonic control on plagioclase weathering in granitic terrain. Earth Planet. Sci. Lett. 301 (3–4), 521–530.
Riebe, C.S., Hahm, W.J., Brantley, S.L., 2017. Controls on deep critical zone architecture: a historical review and four testable hypotheses. Earth Surf. Process. Landf. 42 (1), 128–156.
Riebe, C.S., Kirchner, J.W., Finkel, R.C., 2003. Long-term rates of chemical weathering and physical erosion from cosmogenic nuclides and geochemical mass balance. Geochim. Cosmochim. Acta 67, 4411–4427.
Riebe, C.S., Kirchner, J.W., Finkel, R.C., 2004. Erosional and climatic effects on longterm chemical weathering rates in granitic landscapes spanning diverse climate regimes. Earth Planet. Sci. Lett. 224, 547–562.
Riebe, C.S., Kirchner, J.W., Granger, D.E., Finkel, R.C., 2001. Strong tectonic and weak climatic control of long-term chemical weathering rates. Geology 29, 511–514.
Ross, C.P., 1950. The eastern front of the Bitterroot Range, Montana. U.S. Geol. Survey Bull. 974-E, 135–174, 42p. 44 p.
Shobe, C.M., Tucker, G.E., Anderson, R.S., 2016. Hillslope-derived blocks retard river incision. Geophys. Res. Lett. 43 (10), 5070–5078.
Shobe, C.M., Tucker, G.E., Rossi, M.W., 2018. Variable-threshold behavior in rivers arising from hillslope-derived blocks. J.Geophys.Res.Earth Surf. 123 (8), 1931–1957.
Schoeneberger, P.J., Wysocki, D.A., Benham, E.C., Soil Survey Staff, 2012. Field Book for Describing And Sampling Soils, Version 3.0. Natural Resources Conservation Service, National Soil Survey Center, Lincoln, NE.
Simanton, J.R., Renard, K.G., Christiansen, C.M., Lane, L.J., 1994. Spatial distribution of surface rock fragments along catenas in Semiarid Arizona and Nevada, USA. Catena 23, 29–42.
Sklar, L.S., Riebe, C.S., Marshall, J.A., Genetti, J., Leclere, S., Lukens, C.L., Merces, V., 2017. The problem of predicting the size distribution of sediment supplied by hillslopes to rivers. Geomorphology 15, 31–49.
Stallard, R.F., 1985. River chemistry, geology, geomorphology, and soils in the Amazon and Orinoco Basins. In: Reidel, D., Drever, J.I. (Eds.), The Chemistry of Weathering. Publishing Company, Dordrecht, pp. 293–316.
Stallard, R.F., Edmond, J.M., 1983. Geochemistry of the Amazon 2. The influence of geology and weathering environment on the dissolved load. J. Geophys. Res. 88, 9671–9688.
Stickney, Michael, 2014. New LiDAR data reveals late Quaternary geology details in the Bitterroot Valley, Western Montana. Geological Society of America Rocky Mountain and Cordilleran Sections Joint Meeting, Session No. 27. Montana State University, Bozeman. 21 May, 2014 [dataset].
Taboada, T., Cortizas, A.M., García, C., García-Rodeja, E., 2006. Particle-size fractionation of titanium and zirconium during weathering and pedogenesis of granitic rocks in NW Spain. Geoderma 131 (1–2), 218–236.
Tarboton, 1997. TauDem. Utah State University. http://hydrology.usu.edu/taudem/taudem5, 1997.
Walker, J.C.G., Hays, P.B., Kasting, J.F., 1981. A negative feedback mechanism for the long-term stabilization of the Earth's surface temperature. J. Geophys. Res. 86, 9776–9782.
Weber, W.M., 1972. Correlation of Pleistocene Glaciation in the Bitterroot Range, Montana, With fluctuations of Glacial Lake Missoula. Bureau of Mines and Geology Memoir, Montana, 42p. 44 p.

West, A.J., Galy, A., Bickle, M.J., 2005. Tectonic and climatic controls on silicate weathering. Earth Planet. Sci. Lett. 235, 211–228.
West, A.J., 2012. Thickness of the chemical weathering zone and implications for erosional and climatic drivers of weathering and for carbon-cycle feedbacks. Geology 40, 811–814.
White, A.F., Blum, A.E., 1995. Effects of climate on chemical weathering in watersheds. Geochim. Cosmochim. Acta 59, 1729–1747.
White, A.F., Brantley, S.L., 2003. The effect of time on the experimental and natural weathering rates of silicate minerals. Chem. Geol. 202, 479–506.
Whitlock, C., Bartlein, P.J., 1993. Spatial variations of Holocene climatic change in the Yellowstone region. Quat. Res. 39 (2), 231–238.
Yoo, K., Amundson, R., Heimsath, A.M., Dietrich, W.E., Brimhall, G.H., 2007. Integration of geochemical mass balance with sediment transport to calculate rates of soil chemical weathering and transport on hillslopes. J. Geophys. Res. 112, F02013.